H2Open Journal

IWA PUBLISHING

H2Open Journal Vol 3 No 1
doi: 10.2166/h2oj.2020.021

Delineation of flood-prone areas using modified topographic index for a river basin

D. Nagesh Kumar[a], Apoorva R. Shastry[a] and K. Srinivasa Raju[b,*]

[a] Department of Civil Engineering, Indian Institute of Science, Bangalore 560 012, India

[b] Department of Civil Engineering, Birla Institute of Technology and Science, Pilani-Hyderabad Campus, Hyderabad 500 078, India

*Corresponding author. E-mail: ksraju@hyderabad.bits-pilani.ac.in

Abstract

The modified topographic index (TI_m) based on digital elevation models (DEMs) was employed to delineate flood-prone areas in Mahanadi basin, India. TI_m and flood inundation maps were compared to obtain the threshold (τ) beyond which the area is assumed to be inundated by flood and the exponent of the TI_m. Scale dependence was also investigated to evaluate the sensitiveness of spatial resolution of the DEMs. DEMs of five resolutions, namely, ASTER global, SRTM, GMTED2010 (30 arc-seconds), GMTED 2010 (15 arc-seconds), and GMTED 2010 (7.5 arc-seconds), were used and ASTER global was preferred due to its low error compared to the remainder. Flood frequency analysis was conducted to obtain the relationship between flood-prone areas and flood magnitude. It was observed that (i) the exponent in the TI_m showed little variation, (ii) τ is reduced with reducing spatial resolution of the DEM, and (iii) error is also reduced as the DEMs' resolution is reduced.

Key words: digital elevation models, flood-prone area, frequency analysis, Mahanadi basin, modified topographic index

INTRODUCTION

Flooding is the most frequent hazard worldwide and occurs due to continuous heavy rainfall and failure of hydraulic structures. The impact of floods has increased due to an increase in urbanization and climate change. With the increase in floods, it is important to have effective flood control mechanisms such as afforestation, reduction of deforestation, building flood warning systems. This alarming situation necessitates the creation of flood hazard maps. Clubb *et al.* (2017) opined that hydraulic/flood modeling, even though expected to be informative and helpful, is computationally a burden to the modelers. This is mainly due to the enormous input data requirement, tedious calibration procedures of parameters, and lack of observed data in most of the situations, making the preparation and maintenance of precise flood mapping difficult and expensive. In addition, Sharma *et al.* (2018), as part of their studies on Northeast India, opined that reliance on satellite products is increasing due to insufficient hydrologic gauge stations. These restraints and opportunities suggest simple but effective digital elevation model (DEM)-based approaches that facilitate extraction of topographic-based indices to compute flood inundation area/mapping (Liu & Gupta 2007; Manfreda *et al.* 2008).

H2Open Journal Vol 3 No 1
doi: 10.2166/h2oj.2020.021

The easy availability of surface elevation data has increased the use of DEM-based hydro-geomorphic models. Consequently, more DEM-based methods for delineation of floodplains are used. Elevation of a region, surface slope of the area, distance from the stream, and drainage area are some of the parameters employed to predict the extent of flood inundation. Spatial distribution of the soil moisture and landscape processes can be described by the topographic index (*TI*). Manfreda *et al.* (2008) observed that a strong correlation exists between flood inundation areas and *TI*. Higher *TI* indicates the most susceptible flood-prone areas. Keeping this in mind, the spatial resolution of DEMs is found to be important in obtaining the *TI* (Mukherjee *et al.* 2013; Schumann & Andreadis 2016; Ettritch *et al.* 2018).

The present paper covers a literature review, a brief description of *TI* and modified topographic index (TI_m), study area, analysis of data and methodology, results and discussion, summary and conclusions. The proposed methodology is applied to the Mahanadi River basin, India.

LITERATURE REVIEW

In recent times, many researchers have studied flood modeling, flood simulation, flood management, and flood damage evaluations. With climate change and the increasing impact of floods in urban areas, it becomes important to assess the risk due to natural hazards for planning mitigation measures and management. Hence, the delineation of areas prone to flood inundation is essential. A brief literature review follows.

Flood-prone areas using topographic index

Manfreda *et al.* (2008) evaluated the flood exposure by using morphological indices, namely, local slope, drainage area, curvature, and *TI* for the Arno River basin, Italy. It was observed that the *TI* and local slope show maximum dependency on the flood inundation exposure. TI_m was proposed and used for flood-prone area delineation by identifying the areas which exceeded a given threshold τ. They suggested higher resolution DEMs. Manfreda *et al.* (2011) tested the sensitiveness to DEM spatial resolution by using DEMs of different spatial resolutions for the Arno River basin. It was found that 100 m cell size yielded good performance. Mukherjee *et al.* (2013) carried out *TI* studies on four small watersheds, positioned over the Himalayan terrain. They also explained in detail the computational procedure of specific catchment area, slope, and *TI*. They found that DEM grid spacing significantly affected mean *TI*. Cooper (2014) examined two approaches for Chao Phraya River basin and Bangkok Metropolitan region, Thailand. The first approach handled an up-to-date composite flood hazard map whereas the second explored TI_m for delineating flood-prone areas. He concluded that TI_m is promising. Manfreda *et al.* (2014) employed linear binary classifier, TI_m, and hydrogeomorphic methods to ascertain the potentiality of geomorphic algorithms for preliminary flood hazard graduation and hydraulic risk mapping for two sub-catchments of the Tiber River, central Italy. Simulated flood areas were compared with standard flood maps and it was concluded that the hydrogeomorphic method is effective for ungauged basins. Di Leo *et al.* (2011) emphasized the role of GRASS and QGIS add-ons including r. hazard flood, that uses a TI_m for the flooding delineation.

De Risi *et al.* (2014) studied DEM as well as a probabilistic framework for Ouagadougou, Burkina Faso, Africa for the year 2009. They concluded that the Bayesian updating procedure was useful for computing the topographic wetness index (*TWI*) threshold. Aksoy *et al.* (2016) assessed flood-prone areas in a Turkish watershed and explored the topographical and automated geoscientific analysis of wetness indices. Mattivi *et al.* (2019) compared different open source GIS software for computation of *TWI* for a case study of the Rio Sinigo basin, in northern Italy. Similar studies are reported by Kazakis

H2Open Journal Vol 3 No 1
doi: 10.2166/h2oj.2020.021

et al. (2015) for Rhodope-Evros region, Greece and two specific sites, Cottonwood Lake Study area and Nelson Eddy in Prairie Pothole region, USA.

Marthews *et al.* (2015) expanded upon the importance, necessity, and advantages of *TI* and the limitations. Schumann & Andreadis (2016) discussed the associated economic impacts/benefits achieved in flood prediction in detail and its relevance to society.

Flood-prone areas using other related approaches

Cook & Merwade (2009) evaluated maps from LiDAR data with those obtained by using different geometry, topography, and modeling aspects for Strouds Creek, North Carolina and the Brazos River in Texas. The inundation area was found to be reduced with vertical accuracy in the topographic data and improved with horizontal resolution. Kourgialas & Karatzas (2011) determined flood hazard areas in the Koiliaris River basin, Greece. Rainfall intensity, slope, flow accumulation, geology, land use, and elevation were considered. Degiorgis *et al.* (2013) explored threshold binary classifier techniques for the Tanaro River, Italy for insurance purposes and Samela *et al.* (2016) employed linear binary classifiers to identify flood-prone areas in Africa.

Papaioannou *et al.* (2015) studied a multicriteria perspective for delineation of potential flood-prone areas for the Xerias River watershed, Greece. Zheng *et al.* (2018) performed similar studies on high-resolution terrain analysis for Onion Creek watershed, central Texas.

Distribution functions

Mujere (2011) employed Gumbel distribution for carrying out flood frequency analysis in the Nyanyadi River basin in Zimbabwe. It was hypothesized that the Gumbel distribution would fit the flood flows in the region. An χ^2 test was performed and the recorded and predicted flows provided a good match. The estimates of 100-year and 200-year floods were obtained. Thirty years of maximum instantaneous flood flow data were used for the analysis. Ilorme *et al.* (2014) demonstrated regional rainfall frequency analysis and analysis of ungauged basin to compute discharges in the Gonaives basin, Haiti. Guru & Jha (2015) used peak over threshold flood series and annual maximum (AM) flood series to conduct flood frequency analysis at Kesinga and Kantamal, Tel basin, Mahanadi, India for 1972–2009. Generalized Pareto distribution was found to be suitable for AM flood data series. Kamal *et al.* (2017) conducted frequency analysis for the Ganga River at Haridwar and Garhmukteshwar. Lognormal and Gumbel EV1, respectively, were found suitable for the two locations. Similarly, Bhuyan *et al.* (2010) and Kiran *et al.* (2015) studied the Subernarekha River, India and Gaume (2018) used a Bayesian choice in his study.

In line with the Introduction and literature review, the following objectives were formulated:

- efficacy of TI_m for delineating flood-prone areas;
- evaluate the sensitiveness of the resolution of the DEM data;
- establish relationship between the flood inundated area and the magnitude of the flood.

MODIFIED TOPOGRAPHIC INDEX AND FLOOD-PRONE AREAS' DELINEATION

The topographic index is:

$$TI = Log\left[\frac{\alpha_d}{\tan \beta}\right] \tag{1}$$

H2Open Journal Vol 3 No 1
doi: 10.2166/h2oj.2020.021

where α_d and $\tan\beta$ are, respectively, drained area/unit contour length and local slope (Kirkby 1975). Manfreda *et al.* (2011) modified the TI as:

$$TI_m = Log\left[\frac{\alpha_d^n}{\tan\beta}\right] \tag{2}$$

where n is an exponent with value ≤ 1.7.

TI_m allows delineation of the flood-prone area considering that it is the area characterized by the TI_m exceeding a chosen threshold τ. The TI_m map was compared with a flood inundation map for flood-prone areas' delineation by identifying the areas which had the value of $TI_m > \tau$. To estimate τ and the value of n, two error functions are defined (Manfreda *et al.* 2008, 2011):

$$ER1 = 100 \times \frac{S_{Sim} \cap NS_{TI}}{S_{sim}} \tag{3}$$

$$ER2 = 100 \times \frac{NS_{Sim} \cap S_{TI}}{NS_{sim}} \tag{4}$$

where S_{sim} and S_{TI} are sets of territory predicted as flooded and by TI. NS_{sim} and NS_{TI} are non-flooded regions predicted by hydraulic model and TI. $ER1$ is related to precise identification of flood areas whereas $ER2$ is related to error occurring due to overestimation. The objective function is minimization of $(ER1 + ER2)$ which can be solved iteratively for estimation of τ and n (Manfreda *et al.* 2011).

STUDY AREA

The area of interest considered for the present work is the Mahanadi basin (Figure 1). The study area lies between longitude 80° 30′ and 86° 50′ E and latitude 19° 15′ and 23° 35′ N. The length of the river and the catchment area are 900 km and 141,600 km^2, respectively. Mahanadi flows through Jharkhand, Orissa, Maharashtra, and Chhattisgarh states in an easterly direction. It originates at a place located 6 km from Pharsiya village, Chhattisgarh. The monsoon season starts during the first week of June and continues until October and contributes 90% of the total annual rainfall. Average rainfall is 1,438.1 mm. The climate is sub-tropical. The mean summer and winter temperatures are around 29 °C and 21 °C. More details about Mahanadi River basin are available in Baliarsingh (2000) and Shastry (2013).

Analysis of data and methodology

Data used for the present study are as follows:

1. ASTER global DEM, SRTM DEM, GMTED2010 (30 arc-seconds), GMTED 2010 (15 arc-seconds), GMTED 2010 (7.5 arc-seconds) with respective spatial resolutions of 30.35 m, 92.28 m, 911.19 m, 455.59 m, and 227.80 m.
2. The flood inundation maps for lower portions of Mahanadi basin from National Remote Sensing Centre (NRSC) for flood events of 2006, 2008, and 2011.
3. 68 peaks of inflow hydrograph as well as outflow from reservoir for 1958–1995. More information about data is available in Patri (1993), Baliarsingh (2000), and Nagesh Kumar *et al.* (2010).

Geographical information system (GIS) operations were carried out on the DEMs to obtain all relevant information required for flood inundation maps. Figure 1 was used to obtain the outline of the Mahanadi basin. The map was georeferenced with the help of the *Georeferencing* toolbar in ArcMap. The latitudes and longitudes on the map were used as the reference for georeferencing.

H2Open Journal Vol 3 No 1
doi: 10.2166/h2oj.2020.021

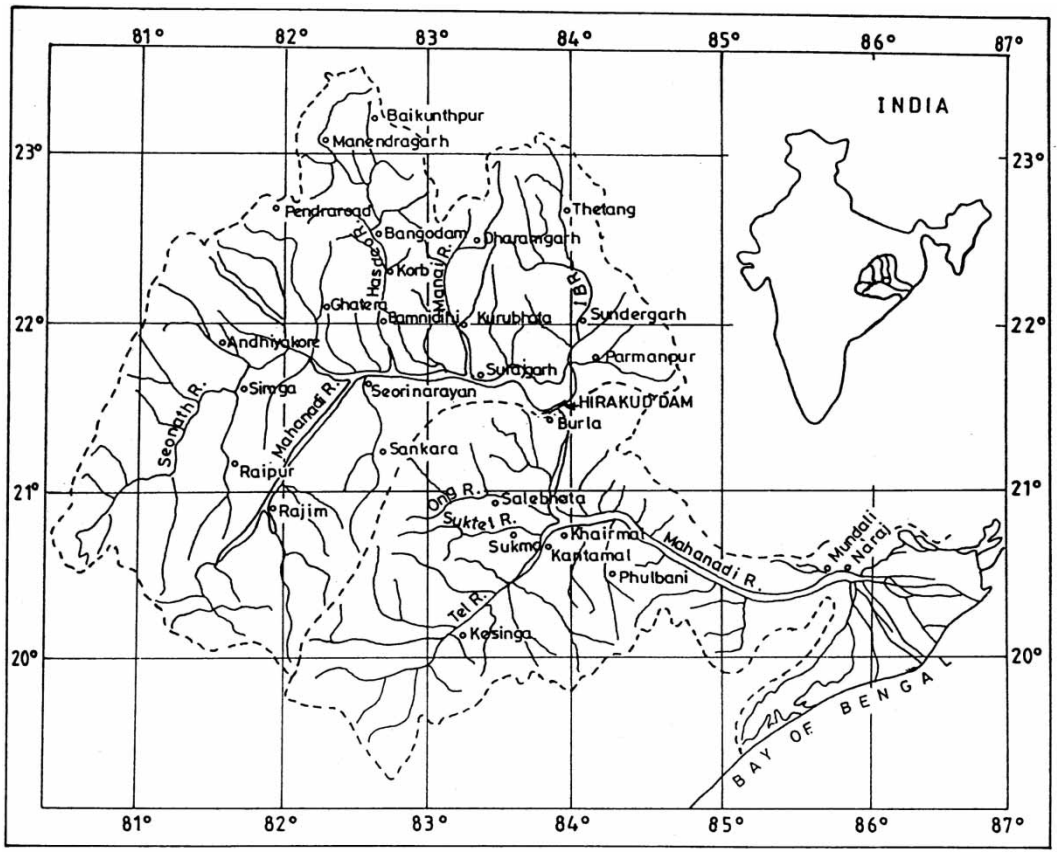

Figure 1 | Map of Mahanadi basin.

Once the map was georegistered, a shape-file of the catchment area was created with the help of the georeferenced map by using the *Editor* toolbar in ArcMap. The shapefile is of polygon type.

The flood inundation maps for three flood events of 2006, 2008, and 2011, were georeferenced using the *Georeferencing* toolbar in ArcMap. The latitudes and longitudes on the map were used as the reference for carrying out the georegistration. The georegistered maps were classified into two classes, i.e., of flooded areas and non-flooded areas. After classification, the areas corresponding to the catchment area present on the maps were selected by superimposing the flood inundation maps over the shape file. The selected area was extracted by using the spatial analyst tool. Once classified maps were obtained, each of these maps was resampled such that the output cell sizes were equal to those of all the DEMs considered in the study, i.e., each of the maps was resampled to have cell sizes 911.19 m, 455.59 m, 227.80 m, 92.28 m, and 30.35 m. Nearest neighbor algorithm was used for resampling such that the flood inundation and TI_m maps would be of the same size for comparison.

The DEMs were processed using ArcMap and MapWindow GIS. To cover the entire Mahanadi basin, a number of DEM tiles of SRTM and ASTER global had to be joined. This was done in ArcMap and processing was done to all the DEMs, i.e., GMTED2010, SRTM, and ASTER global. First, the area corresponding to the flood inundation maps in the Mahanadi basin was extracted using the Arc Toolbox. The extracted flood inundation maps were used to mask and obtain the new image. The DEMs were filled and the filled DEMs were then used to calculate the flow directions. This process takes one input raster, i.e., the filled DEM and produces two output rasters, i.e., Dinf Flow Direction Grid and the Dinf Slope Grid. Specific catchment area is also calculated. The contribution at each grid cell is taken as the grid cell length. This process takes one input raster, the Dinf Flow Direction Raster and produces the specific catchment area raster as the output. The specific catchment area raster and slope raster are used to calculate the TI_m. Iterations are continued

H2Open Journal Vol 3 No 1
doi: 10.2166/h2oj.2020.021

for each value of the exponent to obtain the TI_m. The calculated TI_m is compared to the flood inundation map to calculate $ER1$ and $ER2$. The exponent and the threshold which gives the minimum of the sum of errors $ER1$ and $ER2$ are recorded. Figure 2 presents the procedure involved in arriving at the minimum error, its corresponding exponent and the threshold.

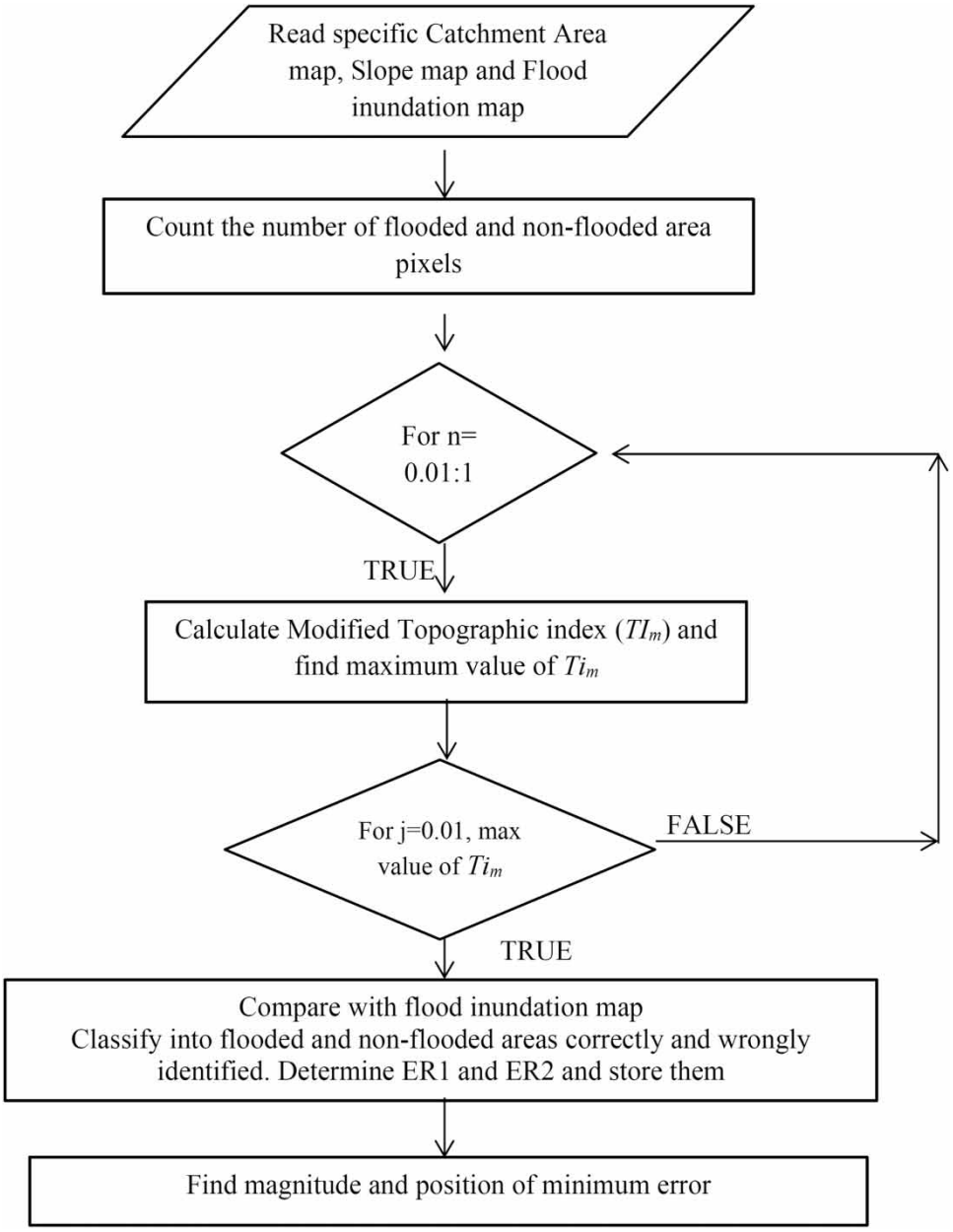

Figure 2 | Procedure for obtaining minimum error, 'n' and 'τ'.

The specific catchment area map, slope map, and the flood inundation map are studied, and from the flooded area map, the count of the number of pixels of flooded area and non-flooded area are calculated. Varying the exponent from 0.01 to 1, TI_m is calculated. Each case of the TI_m is compared with the flood inundation map to obtain a threshold, such that minimum error is obtained while classifying the TI_m map into flooded and non-flooded areas. This is performed by taking a value of TI_m, and classifying all values greater than or equal to it, and if the corresponding pixel in the flood inundation map is flooded area, as correctly identified flooded area, and if the corresponding pixel in flood inundation

H2Open Journal Vol 3 No 1
doi: 10.2166/h2oj.2020.021

map is non-flooded area, as wrongly identified non-flooded area. The wrongly identified flooded and non-flooded area values are used to calculate the error. This procedure is repeated for each value of the TI_m (with an interval of 0.01). The exponent and threshold which produce the minimum error are obtained. They are used to obtain the flood inundation map using ArcMap. While obtaining the flood inundation maps, it is assumed that the entire basin has similar characteristics to that of the test area used in each case of the flood events. The process used to obtain the TI_m map is as follows. The specific catchment area map is first raised to the power of the exponent obtained. Then this image is divided by the slope. The threshold value obtained is used to classify the map into flooded and non-flooded regions. From the created inundation maps, the number of pixels having flooded and non-flooded areas are obtained. Accordingly, the area under flood inundation is calculated and tabulated for all three flood events.

RESULTS AND DISCUSSION

Delineation of flood-prone areas

Table 1 shows the values of n, τ and the corresponding error ($ER1 + ER2$) for the three flood events for all the DEMs.

- It can be seen from Table 1 that the value of n is very low (ranging from 0.01 to 0.04), indicating that the error is minimum when the upslope catchment area has less weightage compared to the downslope. n value of 0.01 is observed for 2011 and 2008 floods for all resolutions.
- The threshold value τ shows a reasonably good trend. These vary from 6.24 to 3.22, 5.49 to 3.22, and 5.27 to 2.87 for 2006, 2011, and 2008 flood events, respectively. The threshold reduced with the reduction in the spatial resolution of the DEM. It can also be seen that as the flood magnitude increased, the threshold has reduced, indicating that a larger area will be under inundation.
- Table 1 also shows the total error. The error also shows a good trend and reduces as spatial resolution of the DEM reduces. It is in agreement with the results that the ideal scale for TI in the case of application in hydrological applications is 10–25 m (Zhang & Montgomery 1994). However, it does not match with the findings of Manfreda *et al.* (2011), where it was found that this method did not provide much improvement with error when the resolution was reduced below 100 m. It was also noted that $ER1$ (the overestimation) was significantly larger than $ER2$ in all the cases and as the DEM resolution is reduced to 30 m, the error reduces drastically.
- Table 1 presents the extent of area inundated by flood in the catchment obtained with the present method for all the five DEMs used. It is observed that ASTER global DEM (30 m) shows a high

Table 1 | Information about three flood events

	n			τ			ER1 + ER2			Inundation area (km^2)		
DEM resolution (m)	2006	2011	2008	2006	2011	2008	2006	2011	2008	2006	2011	2008
900	0.01	0.01	0.01	6.13	5.49	5.27	43.63	37.23	38.70	35,455.73	60,152.03	51,369.46
450	0.04	0.01	0.01	6.24	5.21	5.08	42.63	43.09	39.88	29,045.02	51,366.88	42,633.29
225	0.04	0.01	0.01	5.61	4.78	4.09	39.96	43.97	21.84	35,373.07	75,606.00	48,473.67
90	0.03	0.01	0.01	5.28	4.38	4.32	32.42	37.98	35.51	28,867.16	48,479.82	48,475.09
30	0.01	0.01	0.01	3.22	3.22	2.87	17.40	18.51	18.39	63,670.27	67,251.25	63,670.27
Lowest value among DEMs	0.01	0.01	0.01	3.22	3.22	2.87	17.40	18.51	18.39	28,867.16	48,479.82	42,633.29
Highest value among DEMs	0.04	0.01	0.01	6.24	5.49	5.27	43.63	43.97	39.88	63,670.27	75,606	63,670.27
Difference in highest and lowest values	0.03	0	0	3.02	2.27	2.4	26.23	25.46	21.49	34,803.11	27,126.18	21,036.98

H2Open Journal Vol 3 No 1
doi: 10.2166/h2oj.2020.021

inundation area as compared to other DEMs for 2006 and 2008 flood events and GMTED2010 (225 m) for the 2011 event. It is also noted that GMTED2010 (900 m) and GMTED2010 (225 m) provide approximately the same inundation areas with little difference and, similarly, GMTED2010 (450 m) and SRTM DEM (90 m) for the 2006 event. Similar inferences can be drawn for other events. The differences in the highest and lowest inundation areas obtained by DEMs are also presented in Table 1 and the magnitude of these values are 34,803.11 km^2, 27,126.18 km^2, and 21,036.98 km^2, respectively, which clearly indicates that spatial resolution plays a major role.

The relationships established between discharge (Q in m^3/s) and inundation area (A in km^2) for GMTED 2010 (900), GMTED 2010 (450), GMTED 2010 (225), SRTM, and ASTER, respectively, are $A = -265.94 + 1.234\ Q$, $A = 551.29 + 1.013\ Q$, $A = 38{,}337.13 + 0.371\ Q$, $A = -3{,}239.45 + 1.87\ Q$, and $A = 69{,}494.74 - 0.116\ Q$ with corresponding R^2 values 0.1834, 0.1533, 0.006173, 0.5153, and 0.05942. We observed that R^2 value is low for the three inundation maps considered. However, we wish to bring attention to the fact that on a relative scale, SRTM performed much better compared to all other DEM sources. Note that only three flood inundation maps are used for establishing the relationship for demonstration. We believe that R^2 value will improve if a greater number of flood events are considered in order to develop a robust and sustainable relationship, and this is targeted for further studies.

Flood frequency analysis

All extreme value distribution functions are considered. Among them Gumbel is found to fit well (Odry & Arnaud 2017; Onen & Bagatur 2017; Kobierska *et al.* 2018). Accordingly, the Gumbel method is used for the comparison of flood magnitude and area under flood inundation. It is noted that irrespective of the flood, sufficient and effective infrastructures are required for handling the recurring floods of this magnitude in the catchment. Infrastructure initiatives such as stabilization of slopes, channel regulation, and protection of riverbank and non-structural initiatives such as catchment land management, awareness about insurance facilities, preparedness of emergency management and evacuation, and public education are required and should be implemented in a sustainable manner.

Figure 3 presents the flood inundation map for the year 2011 obtained by incorporating the exponent n and τ with reference to ASTER global for representative purposes. The parameters were computed using a part of the catchment area, and it was assumed that the entire catchment area is similar in behavior. This was performed because the flood inundation map was available only for certain parts of the catchment area. Dark and light shading represent non-flooded area and flooded area, respectively. Figures related to the other four DEMs are not presented here due to the limitation of space. It is a very common phenomenon to study flood magnitude of different recurrence intervals. The flooded area and the non-flooded area on the flood maps provide insight to the officials responsible for flood plain management for remedial/mitigation measures.

SUMMARY AND CONCLUSIONS

In this study, DEMs are used to calculate the TI_m on the basis of which the flood-prone areas are delineated. It was observed that (i) the exponent in the TI_m showed little variation, (ii) τ reduced with reducing spatial resolution of the DEM, and (iii) error also reduced as the DEMs' resolution was reduced. The ASTER provided the best results, and the error is considerably reduced from SRTM

H2Open Journal Vol 3 No 1
doi: 10.2166/h2oj.2020.021

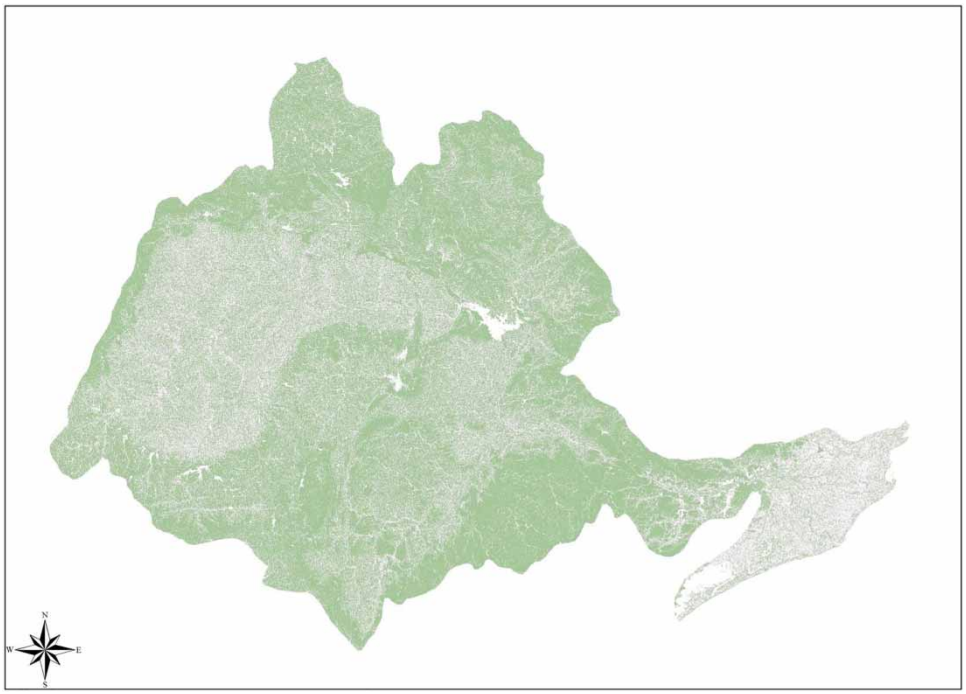

Figure 3 | Inundation map from ASTER DEM for the 2011 flood event.

to ASTER. This is in agreement with the available literature which has found that 10–25 m scale is the best scale for hydraulic applications using the topographic index (Quinn *et al.* 1995).

The present study has a number of similarities and dissimilarities as compared to Manfreda *et al.* (2011). They preferred SRTM for 11 sub-basins of the Arno River basin with 12 cell sizes, whereas the authors of this study suggested ASTER for the Mahanadi River basin in India with five cell sizes by considering three flood events. The highest and lowest values of n, τ, and $ER1 + ER2$ obtained, respectively, are 0.48 and 0.02 (range 0.46), 7.9 and 2.3 (range 5.6), 53.6 and 7.5 (range 46.1) whereas these values obtained by the authors are 0.04 and 0.01 (range 0.03), 6.24 and 2.87 (range 3.37), 43.97 and 17.4 (range 26.57). Compared to the findings of the authors, the ranges obtained by Manfreda *et al.* (2011) are wider, which may be due to the large number of sub-basins and more cell sizes.

To prove the philosophy and to confirm the potentiality of our work, we are using the gauged Mahanadi basin. We want to develop a suitable exponent as a function of basin area and flood magnitude. By analyzing a large number of river basins with the number of flood inundation maps with satisfactory relationship, such a developed relation can be extended to any ungauged basins seamlessly with more confidence.

However, this is an approximate method and cannot be considered as an alternative to detailed hydrologic and hydraulic studies. In our opinion, this is the first case study where potentiality of the methodology suggested by Manfreda and his team is explored for similar Indian conditions.

ACKNOWLEDGEMENTS

This work is supported by Council of Scientific and Industrial Research, New Delhi, through project no. 22(0782)/19/EMR-II dated 24.7.19. The authors are grateful to NRSC, Hyderabad, India for providing flood inundation maps and greatly benefited from Prof. Manfreda and his team's research papers.

H2Open Journal Vol 3 No 1
doi: 10.2166/h2oj.2020.021

REFERENCES

Aksoy, H., Kirca, V. S. O., Burgan, H. I. & Kellecioglu, D. 2016 Hydrological and hydraulic models for determination of flood-prone and flood inundation areas. *Proc. IAHS* **373**, 137–141. doi:10.5194/piahs-373-137-2016.

Baliarsingh, F. 2000 *Long-term and Short-Term Optimal Reservoir Operation for Flood Control*. PhD thesis, Indian Institute of Technology, Kharagpur, India.

Bhuyan, A., Borah, M. & Kumar, R. 2010 Regional flood frequency analysis of North-bank of the River Brahmaputra by using LH-moments. *Water Resour. Manage.* **24** (9), 1779–1790. doi:10.1007/s11269-009-9524-0.

Clubb, F. J., Mudd, S. M., Milodowski, D. T., Valters, D. A., Slater, L. J., Hurst, M. D. & Limaye, A. B. 2017 Geomorphometric delineation of floodplains and terraces from objectively defined topographic thresholds. *Earth Surf. Dyn.* **5**, 369–385. doi:10.5194/esurf-5-369-2017.

Cook, A. & Merwade, V. 2009 Effect of topographic data, geometric configuration and modeling approach on flood inundation mapping. *J. Hydrol.* **377** (1–2), 131–142. doi:10.1016/j.jhydrol.2009.08.015.

Cooper, R. T. 2014 Open data flood mapping of chao phraya river basin and Bangkok metropolitan region. *Br. J. Environ. Clim. Change.* **4** (2), 186–216.

Degiorgis, M., Gnecco, G., Gorni, S., Roth, G., Sanguineti, M. & Taramasso, A. C. 2013 Flood hazard assessment via threshold binary classifiers: case study of The Tanaro River Basin. *Irrig. Drain.* **62** (S2), 1–10. doi:10.1002/ird.1806.

De Risi, R., Jalayer, F., De Paola, F. & Giugni, M. 2014 Probabilistic delineation of flood-prone areas based on a digital elevation model and the extent of historical flooding: the case of Ouagadougou. *Boletín Geológico y Minero* **125** (3), 329–340.

Di Leo, M., Manfreda, S. & Fiorentino, M. 2011 An automated procedure for the detection of flood prone areas: r.hazard.flood. *Geomat. Workb.* **10**, 83–89.

Ettritch, G., Hardy, A., Bojang, L., Cross, D., Bunting, P. & Brewer, P. 2018 Enhancing digital elevation models for hydraulic modelling using flood frequency detection. *Remote Sens. Env.* **217**, 506–522.

Gaume, E. 2018 Flood frequency analysis: the Bayesian choice. *WIREs Water* **5** (4), e1290. doi:10.1002/wat2.1290.

Guru, N. & Jha, R. 2015 Flood frequency analysis of Tel basin of Mahanadi river system India using annual maximum and POT flood data. *Aqua. Proc.* **4**, 427–434. doi:10.1016/j.aqpro.2015.02.057.

Ilorme, F., Griffis, V. & Watkins Jr, D. 2014 Regional rainfall frequency and ungauged basin analysis for flood risk assessment in Haiti. *J. Hydrol. Eng.* **19** (1), 123–132. doi:10.1061/(ASCE)HE.1943-5584.0000757.

Kamal, V., Mukherjee, S., Singh, P., Sen, R., Vishwakarma, C. A., Sajadi, P., Asthana, H. & Rena, V. 2017 Flood frequency analysis of Ganga river at Haridwar and Garhmukteshwar. *Appl. Water Sci.* **7** (4), 1979–1986. doi:10.1007/s13201-016-0378-3.

Kazakis, N., Kougias, I. & Patsialis, T. 2015 Assessment of flood hazard areas at a regional scale using an index-based approach and analytical hierarchy process: application in Rhodope–Evros region, Greece. *Sci. Tot. Env.* **538**, 555–563. doi:10.1016/j.scitotenv.2015.08.055.

Kiran, Y., Samanta, B. & Deb, D. 2015 L-moment and composite model approaches for regional flood frequency analysis. *Int. J. Hydrol. Sci. Tech.* **5** (2), 95–118. doi:10.1504/IJHST.2015.070097.

Kirkby, M. J. 1975 Hydrograph modelling strategies. In: *Progress in Physical and Human Geography* (Peel, R. F., Chisholm, M. D. & Haggett, P., eds). Heinemann, London, UK, pp. 69–90.

Kobierska, F., Engeland, K. & Thorarinsdottir, T. 2018 Evaluation of design flood estimates – a case study for Norway. *Hydrol. Res.* **49** (2), 450–465. doi:10.2166/nh.2017.068.

Kourgialas, N. N. & Karatzas, G. P. 2011 Flood management and a GIS modelling method to assess flood-hazard areas – a case study. *Hyd. Sci. J.* **56** (2), 212–225. doi:10.1080/02626667.2011.555836.

Liu, Y. & Gupta, H. V. 2007 Uncertainty in hydrologic modeling: toward an integrated data assimilation framework. *Water Resour. Res.* **43**, W07401. doi:10.1029/2006WR005756.

Manfreda, S., Nardi, F., Samela, C., Grimaldi, S., Taramasso, A. C., Roth, G. & Sole, A. 2014 Investigation on the use of geomorphic approaches for the delineation of flood prone areas. *J. Hydrol.* **517**, 863–876. doi:10.1016/j.jhydrol.2014.06.009.

Manfreda, S., Sole, A. & Fiorentino, M. 2008 Can the basin morphology alone provide an insight on floodplain delineation? *WIT Trans. Eco. Envir.* **118**, 47–56. doi:10.2495/FRIAR080051.

Manfreda, S., Sole, A. & Leo, M. D. 2011 Detection of flood prone areas using digital elevation models. *J. Hydrol. Eng.* **16** (10), 781–790. doi:10.1061/(ASCE)HE.1943-5584.0000367.

Marthews, T. R., Dadson, S. J., Lehner, B., Abele, S. & Gedney, N. 2015 High-resolution global topographic index values for use in large-scale hydrological modelling. *Hydrol. Earth Syst. Sci.* **19**, 91–104.

Mattivi, P., Franci, F., Lambertini, A. & Bitelli, G. 2019 TWI computation: a comparison of different open source GISs. *Open Geospat. Data, Softw. Stand.* **4** (1), 1–12. doi:10.1186/s40965-019-0066-y.

Mujere, N. 2011 Flood frequency analysis using the Gumbel distribution. *Int. J. Comp. Sci. Eng.* **3** (7), 2774–2778.

Mukherjee, S., Mukherjee, S., Garg, R. D., Bhardwaj, A. & Raju, P. L. N. 2013 Evaluation of topographic index in relation to terrain roughness and DEM grid spacing. *J. Earth Syst. Sci.* **122** (3), 869–886.

Nagesh Kumar, D., Baliarsingh, F. & Srinivasa Raju, K. 2010 Optimal reservoir operation for flood control using folded dynamic programming. *Water Resour. Manage.* **24** (6), 1045–1064. doi:10.1007/s11269-009-9485-3.

Odry, J. & Arnaud, P. 2017 Comparison of flood frequency analysis methods for ungauged catchments in France. *Geosciences* **7**, 88. doi:10.3390/geosciences7030088.

Onen, F. & Bagatur, T. 2017 Prediction of flood frequency factor for Gumbel distribution using regression and GEP model. *Arab J. Sci. Eng.* **42** (9), 3895–3906. doi:10.1007/s13369-017-2507-1.

H$_2$Open Journal Vol 3 No 1
doi: 10.2166/h2oj.2020.021

Papaioannou, G., Vasiliades, L. & Loukas, A. 2015 Multi-criteria analysis framework for potential flood prone areas mapping. *Water Resour. Manage.* **29** (2), 399–418. doi:10.1007/s11269-014-0817-6.

Patri, S. 1993 *Data on Flood Control Operation of Hirakud Dam*. Irrigation Department, Government of Orissa, India, p. 200.

Quinn, P. F., Beven, K. J. & Lamb, R. 1995 The in(a/tan/β) index: how to calculate it and how to use it within the topmodel framework. *Hydrol. Process.* **9** (2), 161–182.

Samela, C., Manfreda, S., Paola, F., Giugni, M., Sole, A. & Fiorentino, M. 2016 DEM-based approaches for the delineation of flood-prone areas in an ungauged basin in Africa. *J. Hydrol. Eng.* **21** (2). doi:10.1061/(ASCE)HE.1943-5584.0001272.

Schumann, G. J. P. & Andreadis, K. M. 2016 A method to assess localized impact of better floodplain topography on flood risk prediction. *Adv. Meteorol.* doi:10.1155/2016/6408319.

Sharma, S. K., Kwak, Y. J., Kumar, R. & Sarma, B. 2018 Analysis of hydrological sensitivity for flood risk assessment. *ISPRS Int. J. Geo-Inf.* **7**, 51. doi:10.3390/ijgi7020051.

Shastry, A. R. 2013 Delineation of Flood-Prone Areas Using Modified Topographic Index for Mahanadi Basin. ME thesis, Indian Institute of Science, Bangalore, India.

Zhang, W. & Montgomery, D. R. 1994 Digital elevation model grid size, landscape representation, and hydrologic simulations. *Water Resour. Res.* **30** (4), 1019–1028. doi:10.1029/93WR03553.

Zheng, X., Maidment, D. R., Tarboton, D. G., Liu, Y. Y. & Passalacqua, P. 2018 Geoflood: large-scale flood inundation mapping based on high-resolution terrain analysis. *Water Resour. Res.* **54** (12), 10013–10033. doi:10.1029/2018WR023457.

First received 10 October 2019; accepted in revised form 27 January 2020. Available online 19 March 2020